Available online at www.sciencedirect.com

ScienceDirect

Mendeleev Commun., 2021, **31**, 784–788

Mendeleev Communications

Novel organic magnet derived from pyrazine-fused furazans

Victor I. Ovcharenko,*[a,b] Aleksei B. Sheremetev,[a] Kirill V. Strizhenko,[a] Sergey V. Fokin,[b] Galina V. Romanenko,[b] Artem S. Bogomyakov,[a,b] Vitaly A. Morozov,[b] Mikhail A. Syroeshkin,[a] Anna Ya. Kozmenkova,[a] Andrey V. Lalov[a] and Mikhail P. Egorov*[a]

[a] *N. D. Zelinsky Institute of Organic Chemistry, Russian Academy of Sciences, 119991 Moscow, Russian Federation. E-mail: mpe@ioc.ac.ru*

[b] *International Tomography Center, Siberian Branch of the Russian Academy of Sciences, 630090 Novosibirsk, Russian Federation. E-mail: Victor.Ovcharenko@tomo.nsc.ru*

DOI: 10.1016/j.mencom.2021.11.005

The first organic magnet based on a high-nitrogen framework of pyrazine-fused furazans $Na(L^{\bullet-})(H_2O)_3$ was found. A quantum-chemical study of $M(L^{\bullet-})(H_2O)_n$, where M = Li, Na, K, Rb, NH_4, revealed that exchange coupling energy between the neighboring radical anions proved highly sensitive to the motion of one $L^{\bullet-}$ relative to another.

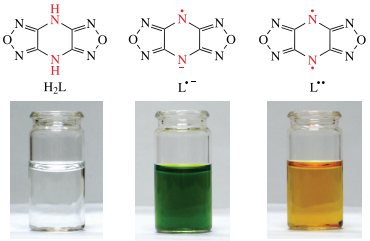

Keywords: bis(furazano)pyrazine, sodium, potassium, rubidium, ammonium, stable radical, molecular magnet, McConnell's exchange model.

Stable organic radicals have been of great academic interest not only in the context of fundamental understanding of reactive intermediates but also because of their numerous applications as functional materials.[1–7] An intriguing idea is to create new types of magnetically active compounds saturated with organic components based on synthetic chemistry approaches. This would impart them the properties typical of organic compounds: low density, elasticity, transparency over a broad range of electromagnetic spectrum, high resistance to electric current, biocompatibility.[8–10] Miller drew attention to the fact that molecule-based magnets and their precursors are frequently soluble in conventional organic solvents and do not require energy intensive metallurgical preparative methods.[11] Persistent organic radicals are considered to be promising building blocks for multi-functional molecule-based magnetic materials and the design of different devices.[3,12–17] These radicals have emerged as promising compounds for organic spintronics,[18–20] memory devices,[21–24] spin sensors,[25] spin filters,[26,27] probing quantum interference effects in molecular conductance,[28,29] gaseous separation of small paramagnetic molecules[30] and magnetically driven micro and nanorobots.[31]

However, reliably and reproducibly recorded bulk magnetic ordering for organic compounds is an extremely rare event.[11,12,32–36] The structures of some of these compounds are shown in Figure 1.

Note that the solid phases of these compounds are often amorphous, which creates problems in studies of magneto-structural correlations, or possess extremely low magnetization and high sensitivity to oxygen or air moisture. These circumstances stimulate active search for novel organic radical platform of highly stable organic radicals[7] possessing a new set of physicochemical properties, which may be useful for studies in the field of molecular/organic magnets.[11]

Here, a new type of highly stable radical derived from pyrazine-fused furazans is described. This air- and water-stable radical was found among the products of oxidation of the tricyclic heterocyclic compound, *viz.* 4*H*,8*H*-bis(furazano)[3,4-*b*:3′,4′-*e*]-pyrazine (H_2L, Figure 2), previously investigated only in the chemistry of energetic materials.[37–54] Earlier, it was noted only that the oxidation of H_2L with powerful oxidants (anhydrous nitric acid, fluorine, chlorine, or hot Caro's acid) could form radical species.[38,41] We found that weaker oxidants could be used for the oxidation of H_2L, especially in alkaline media, and as oxidants we chose PbO_2 powder and Br_2 gas (see Online Supplementary Materials). The oxidation of H_2L was carried out under heterophase conditions in both cases; due to this, the oxidation could be easily stopped by filtering off PbO_2 or blocking

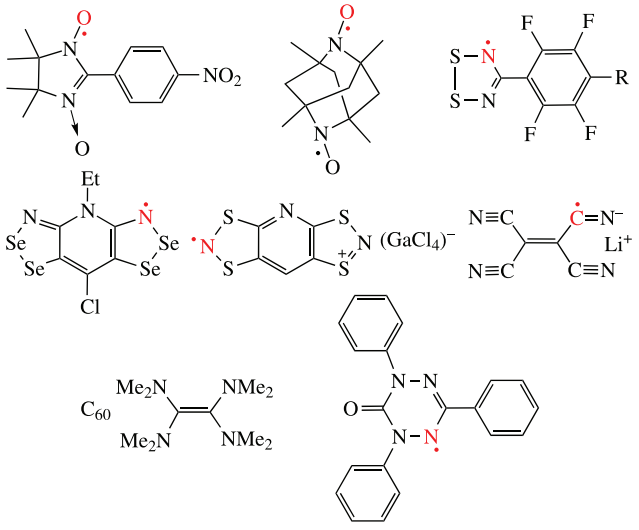

Figure 1 Organic molecular magnets.

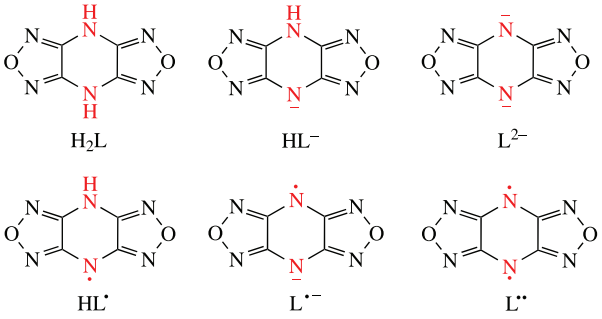

Figure 2 H_2L, HL^-, L^{2-}, $L^{\bullet-}$, $HL^{\bullet}$, and $L^{\bullet\bullet}$ molecules.

the access of bromine vapor to the surface of the reaction mixture. Figure 3 briefly illustrates the results of an electrochemical study showing that the products of dissociation of H_2L and HL^-, whose contents drastically increase after the addition of a strong base to the reaction medium, are oxidized more readily than H_2L.

The oxidation of H_2L is conveniently performed in water as aqueous solutions of paramagnetic polycyclic pyrazines are kinetically persistent under normal conditions for a long time sufficient to grow high-quality $M(L^{\bullet-})(H_2O)_n$ single crystals. However, well-resolved EPR spectra of radical species are more conveniently recorded in organic solvents. Figure 4 gives examples of the experimental and theoretical spectra of the radical anion recorded at a potential of 0.8 V in a two-electrode Pt/Pt electrochemical cell placed in a resonator of an EPR spectrometer. The results of spectrum simulation agree well with the data of the quantum-chemical calculation of the HFC constants for $L^{\bullet-}$, namely, $g_i = 2.0058$, a_N (4*N*, 8*N*) = 0.4 mT, a_N (1*N*, 3*N*, 5*N*, 7*N*) = 0.14 mT.

Salts $NH_4(L^{\bullet-})(H_2O)_3$, $Na(L^{\bullet-})(H_2O)_3$, $K(L^{\bullet-})(H_2O)_{2.5}$ and $Rb(L^{\bullet-})(H_2O)$ were obtained using the PbO_2 oxidant. For the synthesis of $Li(L^{\bullet-})(H_2O)_3$ and $L^{\bullet\bullet}$, the oxidation was performed with Br_2 vapors. The reaction mixture should be vigorously

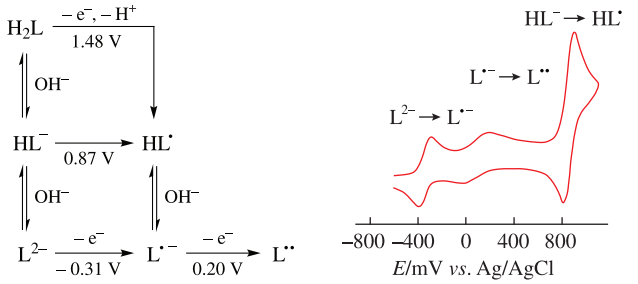

Figure 3 Electrochemical potentials of H_2L, HL^- and L^{2-}; CV curve obtained in 0.1 M Bu_4NBF_4/MeCN on a glassy carbon electrode (see Online Supplementary Materials, Section 2 for details).

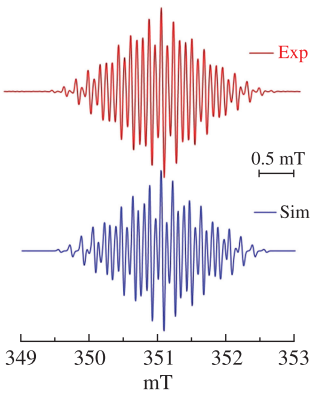

Figure 4 EPR spectra of $L^{\bullet-}$: experimental (red line; THF/Bu_4NClO_4/+0.8 V) and simulated (blue line, $g_i = 2.0059$, $a_N = 0.42$ mT, $a_N = 0.16$ mT, LW = 0.04 mT).

stirred, limiting the contact time between the solution surface and the Br_2 vapors in order to avoid the oxidation of $L^{\bullet-}$ to $L^{\bullet\bullet}$. Unlike colorless H_2L solutions, $L^{\bullet-}$ and $L^{\bullet\bullet}$ solutions are colored bright green and brown (see movie in Online Supplementary Materials), respectively, which makes them easy to visualize when they appear in the reaction mixture. The oxidation potentials of H_2L in different solvents are close (see Online Supplementary Materials).

Our study of the magnetic properties of the compounds revealed that $Na(L^{\bullet-})(H_2O)_3$ underwent magnetic ordering at low temperatures. This result was reliably reproduced and did not depend on any peculiarities of the synthetic procedure. For other $M(L^{\bullet-})(H_2O)_n$, where M = Li, K, Rb, NH_4, bulk magnetic ordering was not recorded. $L^{\bullet\bullet}$ is diamagnetic, which is fully consistent with the results of our quantum-chemical study (the ST gap for the $L^{\bullet\bullet}$ molecule is ~6100 cm^{-1}).

The field dependences of magnetization for $Na(L^{\bullet-})(H_2O)_3$ at 2, 3, and 4 K are presented in Figure 5. Magnetization increases sharply with the magnetic field strength; above 7 kOe, it increases monotonically. An analysis of the $M(H)$ dependences using the equation $M = M_0 + xH$ made it possible to evaluate spontaneous magnetization M_0 and magnetic susceptibility (see Online Supplementary Materials). Figure 5 also gives the temperature dependence of magnetization of the compound in a magnetic field of H = 200 Oe, which shows that magnetization drastically increases below 4.5 K.

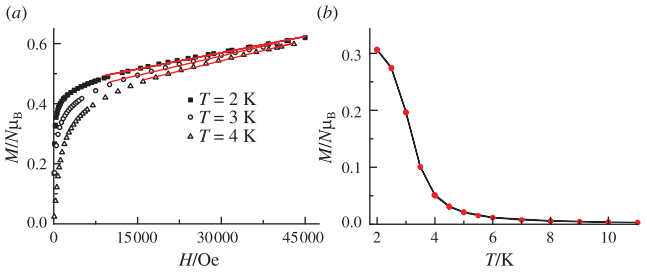

Figure 5 For $Na(L^{\bullet-})(H_2O)_3$: (*a*) dependence of M on H at different temperatures; (*b*) dependence of M on T at H = 200 Oe.

† *Crystal data for* H_2L.[39] $C_4H_2N_6O_2$, $F_W = 166.00$, $T = 110$ K, space group $P2_1/n$, $Z = 2$, $a = 5.1253(1)$, $b = 4.4839(1)$ and $c = 11.8178(3)$ Å, $\beta = 91.072(1)°$, $V = 271.54(1)$ Å^3, $D_{calc} = 2.032$ g cm^{-3}.

Crystal data for $H_2L{\cdot}2DMF$. $C_{10}H_{16}N_8O_4$, $F_W = 312.31$, $T = 296$ K, space group $C2/c$, $Z = 4$, $a = 21.1751(12)$, $b = 4.1239(2)$ and $c = 18.4848(10)$ Å, $\beta = 115.567(2)°$, $V = 1456.11(14)$ Å^3, $D_{calc} = 1.425$ g cm^{-3}.

Crystal data for $(NH_4)(L^{\bullet-})(H_2O)_3$. $C_4H_{10}N_7O_5$, $F_W = 234.20$, $T = 296$ K, space group $P2_1/c$, $Z = 4$, $a = 8.6393(6)$, $b = 6.7123(5)$ and $c = 8.8415(6)$ Å, $\beta = 103.154(5)°$, $V = 499.26(6)$ Å^3, $D_{calc} = 1.574$ g cm^{-3}.

Crystal data for $L^{\bullet\bullet}$. $C_4N_6O_2$, $F_W = 164.10$, $T = 296$ K, space group *Cmca*, $Z = 4$, $a = 15.935(4)$, $b = 5.6876(14)$ and $c = 6.6326(18)$ Å, $V = 601.1(3)$ Å^3, $D_{calc} = 1.813$ g cm^{-3}.

Crystal data for $Li(L^{\bullet-})(H_2O)_3$. $C_4H_6LiN_6O_5$, $F_W = 225.09$, $T = 296$ K, space group *Cc*, $Z = 4$, $a = 16.4101(5)$, $b = 6.4572(2)$ and $c = 8.6603(3)$ Å, $\beta = 104.164(2)°$, $V = 889.78(5)$ Å^3, $D_{calc} = 1.680$ g cm^{-3}.

Crystal data for $Na(L^{\bullet-})(H_2O)_3$. $C_4H_6N_6NaO_5$, $F_W = 241.14$, $T = 296$ K, space group $P\bar{1}$, $Z = 2$, $a = 3.5452(5)$, $b = 8.0940(9)$ and $c = 16.206(2)$ Å, $\alpha = 102.815(9)°$, $\beta = 94.891(10)°$, $\gamma = 90.540(9)°$, $V = 451.60(10)$ Å^3, $D_{calc} = 1.773$ g cm^{-3}.

Crystal data for $K(L^{\bullet-})(H_2O)_{2.5}$. $C_4H_5KN_6O_{4.5}$, $F_W = 248.24$, $T = 283$ K, space group $C2/c$, $Z = 8$, $a = 22.6136(10)$, $b = 4.0120(2)$ and $c = 20.2128(9)$ Å, $\beta = 94.951(2)°$, $V = 1826.98(15)$ Å^3, $D_{calc} = 1.805$ g cm^{-3}.

Crystal data for $Rb(L^{\bullet-})(H_2O)$. $C_4H_2N_6O_3Rb$, $F_W = 267.58$, $T = 296$ K, space group $P\bar{1}$, $Z = 2$, $a = 13.4013(5)$, $b = 6.7965(3)$ and $c = 9.5489(3)$ Å, $\alpha = 69.178(2)°$, $\beta = 85.648(2)°$, $\gamma = 77.650(2)°$, $V = 794.12(5)$ Å^3, $D_{calc} = 2.238$ g cm^{-3}.

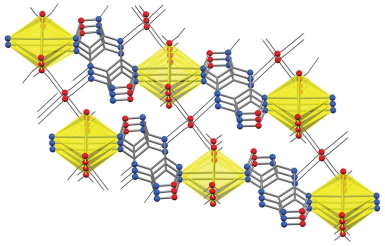

Figure 6 Fragment of the structure of $Na(L^{\bullet-})(H_2O)_3$.

For $M(L^{\bullet-})(H_2O)_n$, there is a large amount of structural information† (see Online Supplementary Materials). Figure 6 shows only a fragment of the structure of $Na(L^{\bullet-})(H_2O)_3$; in the figure, the (yellow) columns of Na atoms surrounded by the O atoms of H_2O molecules and the N atoms of the furazan rings separate the columns of $L^{\bullet-}$ radical anions situated one over another. As the columns of $L^{\bullet-}$ radical anions form a structural motif common to all $M(L^{\bullet-})(H_2O)_n$, the question arises: Why is it only $Na(L^{\bullet-})(H_2O)_3$ that is liable to bulk magnetic ordering of all $M(L^{\bullet-})(H_2O)_n$'s? According to our knowledge, this problem has never appeared in the history of studies on organic magnets. This is probably due to the fact that the ability to undergo cooperative magnetic ordering among organic alkali salts was recorded only once.[55]

Comparative quantum-chemical analysis of magnetostructural correlations inherent in $M(L^{\bullet-})(H_2O)_n$ (Table 1), revealed a high sensitivity of exchange coupling energy among the neighboring radical anions when one $L^{\bullet-}$ moved relative to another $L^{\bullet-}$ in parallel planes (insert, Figure 7). Table 1 shows two different values of J in those cases when the packing of $M(L^{\bullet-})(H_2O)_n$ contains columns of two different types of $L^{\bullet-}$. The exchange between the paramagnetic anions of neighboring columns is insignificant and does not exceed 1–2 cm^{-1}. In the case of $Rb(L^{\bullet-})(H_2O)$, the exchange integrals between the radicals of the neighboring columns are even smaller (<0.1 cm^{-1}).

To describe the revealed effect, which allows us to explain the difference in the magnetic properties of $Na(L^{\bullet-})(H_2O)_3$ from other $M(L^{\bullet-})(H_2O)_n$ salts (M = Li, K, Rb, NH_4), it was useful to construct a special 'orientation–energy' map of exchange interactions (see Figure 7). This map reflects the dynamics of the sign of exchange integral between two adjacent $L^{\bullet-}$'s during the imitated 'flotation' of one species over the other in a parallel plane at a fixed interplanar distance.

Table 1 Magnetic exchange coupling constants J (cm^{-1}).

Compound	LC-BLYP	cam-B3LYP	PBE+U
$Li(L^{\bullet-})(H_2O)_3$	–41.7, –27.8	–44.3, –30.5	–102.0
$Na(L^{\bullet-})(H_2O)_3$	58.3, 58.7	56.7, 55.9	19.3
$K(L^{\bullet-})(H_2O)_{2.5}$	–130.3	–136.4	–103.8
$Rb(L^{\bullet-})(H_2O)$	–48.7, –58.4	–53.0, –57.7	–52.0, –70.0
$NH_4(L^{\bullet-})(H_2O)_3$	–43.2	–44.9	–46.5

The crystals suitable for an XRD analysis were mostly collected directly from the mother solution and immersed into epoxide resin for protection from medium effects. Data sets were obtained on Bruker AXS – SMART APEX II and Apex Duo diffractometers (absorption correction and scaling was done using SADABS program, ver. 2.10). The structures were solved by direct methods and refined by full-matrix least squares anisotropically for all non-hydrogen atoms. For the majority of structures, the positions of H atoms were located in series of electron density syntheses and refined in an isotropic approximation without any restrictions. In some cases, they were calculated geometrically and refined in a riding model with free thermal parameters. All calculations on structure solution and refinement were performed with the Bruker SHELXTL (ver. 6.14) and SHELX set of programs.[58]

CCDC 2081748–2081753 contain the supplementary crystallographic data for this paper. These data can be obtained free of charge from The Cambridge Crystallographic Data Centre *via* http://www.ccdc.cam.ac.uk.

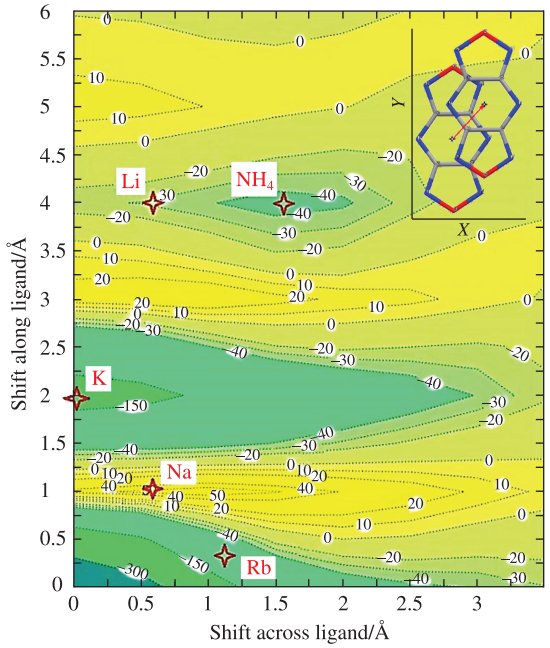

Figure 7 Calculated map of the sign of exchange integral for a pair of $L^{\bullet-}$ radical anions depending on the relative shift of their centers. Light green (turquoise, then green, and then petrol blue at increased exchange energy): regions of antiferromagnetic exchange; yellow: regions of ferromagnetic exchange. Numbers at isolines: values of exchange integrals in cm^{-1}. Red asterisks: points corresponding to $M(L^{\bullet-})(H_2O)_n$, where M = Li, K, Rb, NH_4. Insert: the vector connecting the centers of radical anions demonstrates the relative shift of the neighboring $L^{\bullet-}$ radical anions.

The data of Table 1 show that the values of exchange integrals do not differ significantly for molecular and periodic DFT calculations. As mentioned above, the columnar structure of the paramagnetic anions spaced about 3.2 Å apart is a structural feature common to all $M(L^{\bullet-})(H_2O)_n$ salts. The difference lies in the relative shift of the centers of adjacent radical anions relative to one another (in the insert in Figure 7, the shift is marked by a red vector). It appeared that this shift determines the magnitude and character of exchange interaction in the $L^{\bullet-}$ columns, which was confirmed by the molecular DFT calculation of exchange integrals for a wide set of the relative shifts of ligands along the X and Y axes (see Figure 7).

In the map, the regions of positive exchange integrals are yellow, and those of the negative integrals are green. The points that formally correspond to the relative shifts of ligands for $M(L^{\bullet-})(H_2O)_n$ are also marked in the map. It can be seen that the map gives adequate values and signs of exchange integrals. The map of the sign of exchange integral for a pair of $L^{\bullet-}$ radical anions lying at a distance of 3.2 Å in the parallel planes was calculated for the chosen 2D variant. It can certainly be obtained as a 3D image, although in reality the interplanar distances in these compounds can be decreased by no more than 0.2 Å (see Online Supplementary Materials).

It should also be stressed that the results proved to be perfect experimental support of McConnell-I exchange model.[56] The high sensitivity of exchange coupling energy among the neighboring radical anions when one $L^{\bullet-}$ moved relative to another $L^{\bullet-}$ in parallel planes (insert, Figure 7) is determined by the character of spin density distribution in $L^{\bullet-}$. Indeed, according to the known McConnell-I mode,[56] one would expect antiferro-

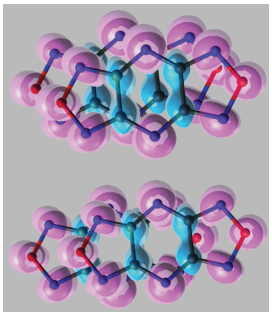

Figure 8 Scheme of spin density overlap of the pair of radical anions $L^{\bullet-}$ in $Na(L^{\bullet-})(H_2O)_3$ with FM exchange integral (top) and in $K(L^{\bullet-})(H_2O)_{2.5}$ with AFM exchange integral (bottom). Top view. Pink: positive spin density, blue: negative spin density; spin density surfaces of the level of 0.002 are shown.

magnetic (AFM) exchange coupling in the $L^{\bullet-}$ pair with significant overlap of spin densities of the same sign and ferromagnetic (FM) exchange coupling with significant overlap of spin densities of opposite signs.

Figure 7 qualitatively confirms this correlation. Thus, the region of the ferromagnetic exchange integral of 40–50 cm^{-1} in Figure 7 corresponds to a relative shift of the centers of radical anions $L^{\bullet-}$ by ~1 Å on both axes. With this shift, the positive spin densities of N atoms overlap the negative spin densities on C atoms most effectively. This situation is close to the relative geometry of arrangement of radical anions in $Na(L^{\bullet-})(H_2O)_3$ (upper panel in Figure 8). The lower panel in Figure 8 corresponds to the relative geometry of arrangement of $L^{\bullet-}$ in $K(L^{\bullet-})(H_2O)_{2.5}$, which is demonstrated by the AFM exchange integral. Although the McConnell-I model is often criticized,[57] in our case it adequately describes the experimental correlations between the exchange sign and the relative arrangement of $L^{\bullet-}$ radical anions in $M(L^{\bullet-})(H_2O)_n$ solids.

In conclusion, the novel family of highly stable paramagnetic organic salts $M(L^{\bullet-})(H_2O)_n$ have been synthesized. Their structure was unambiguously confirmed by X-ray crystallography. We revealed a novel organic magnet, which is a radical anion derivative of bis(furazano)pyrazine, known but poorly understood tricyclic framework. Paramagnetic derivatives of polycyclic furazanopyrazines are also of interest from the viewpoint of a quantum-chemical research, which was confirmed by the results of the investigation of exchange interactions in $M(L^{\bullet-})(H_2O)_n$. The calculated map of the sign of exchange integral for a pair of $L^{\bullet-}$ radical anions lying in parallel planes allowed us to explain the presence of ferromagnetic exchange in $Na(L^{\bullet-})(H_2O)_3$. The results of this study show that careful selection of substrates among high nitrogen compounds can lead to the discovery of new molecular magnets.

This study was financially supported by the Ministry of Science and Higher Education of the Russian Federation (agreement with IOC RAS no. 075-15-2020-803).

Online Supplementary Materials

Supplementary data associated with this article can be found in the online version at doi: 10.1016/j.mencom.2021.11.005.

References

1 *Organic Chemistry of Stable Free Radicals*, eds. A. R. Forrester, J. M. Hay and R. H. Thompson, Academic Press, London, 1968.
2 L. B. Volodarsky, V. A. Reznikov and V. I. Ovcharenko, *Synthetic Chemistry of Stable Nitroxides*, 1st edn., CRC Press, Boca Raton, 2017.
3 H. Robin, *Stable Radicals: Fundamentals and Applied Aspects of Odd-Electron Compounds*, ed. R. G. Hicks, John Wiley & Sons, Ltd., Chichester, 2010.
4 G. I. Likhtenshtein, *Nitroxides: Brief History, Fundamentals, and Recent Developments* (*Springer Series in Materials Science*, vol. 292), 1st edn., Springer International Publishing, Cham, 2020.
5 J. F. W. Keana, *Chem. Rev.*, 1978, **78**, 37.
6 S. N. Datta, C. O. Trindle and F. Illas, *Theoretical and Computational Aspects of Magnetic Organic Molecules*, Imperial College Press, London, 2014.
7 Y. Kim, J. E. Byeon, G. Y. Jeong, S. S. Kim, H. Song and E. Lee, *J. Am. Chem. Soc.*, 2021, **143**, 8527.
8 E. V. Tretyakov and V. I. Ovcharenko, *Russ. Chem. Rev.*, 2009, **78**, 971 (*Usp. Khim.*, 2009, **78**, 1051).
9 S. Suzuki and K. Okada, in *Organic Redox Systems: Synthesis, Properties, and Applications*, ed. T. Nishinaga, Wiley, Hoboken, 2016, pp. 269–285.
10 M. T. Lemaire, *Pure Appl. Chem.*, 2011, **83**, 141.
11 J. S. Miller, *Mater. Today*, 2014, **17**, 224.
12 M. Baumgarten, in *World Scientific Reference on Spin in Organics*, ed. J. S. Miller, World Scientific Publishing, Singapore, 2018, vol. 4, pp. 1–93.
13 M. Abe, *Chem. Rev.*, 2013, **113**, 7011.
14 K. Inoue, in *π-Electron Magnetism: From Molecules to Magnetic Materials*, ed. J. Veciana, Springer, Berlin, Heidelberg, 2001, pp. 61–91.
15 I. Fidan, E. Önal, Y. Yerli, D. Luneau, V. Ahsen and C. Hirel, *ChemPlusChem*, 2017, **82**, 1384.
16 *Organic Redox Systems*: *Synthesis, Properties, and Applications*, ed. T. Nishinaga, Wiley, Hoboken, 2016.
17 E. Coronado and A. J. Epstein, *J. Mater. Chem.*, 2009, **19**, 1670.
18 S. Sanvito, *Chem. Soc. Rev.*, 2011, **40**, 3336.
19 E. Coronado, *Nat. Rev. Mater.*, 2020, **5**, 87.
20 W. Han, K. Pi, K. M. McCreary, Y. Li, J. J. I. Wong, A. G. Swartz and R. K. Kawakami, *Phys. Rev. Lett.*, 2010, **105**, 167202.
21 Y. Yonekuta, K. Susuki, K. Oyaizu and K. Honda, *J. Am. Chem. Soc.*, 2007, **129**, 14128.
22 K. Oyaizu and H. Nishide, *Adv. Mater.*, 2009, **21**, 2339.
23 J. Lee, E. Lee, S. Kim, G. S. Bang, D. A. Shultz, R. D. Schmidt, M. D. E. Forbes and H. Lee, *Angew. Chem., Int. Ed.*, 2011, **50**, 4414.
24 R. Gaudenzi, J. de Bruijckere, D. Reta, I. de P. R. Moreira, C. Rovira, J. Veciana, H. S. J. van der Zant and E. Burzurí, *ACS Nano*, 2017, **11**, 5879.
25 R. Gaudenzi, E. Burzurí, D. Reta, I. de P. R. Moreira, S. T. Bromley, C. Rovira, J. Veciana and H. S. J. van der Zant, *Nano Lett.*, 2016, **16**, 2066.
26 C. Herrmann, G. C. Solomon and M. A. Ratner, *J. Am. Chem. Soc.*, 2010, **132**, 3682.
27 G. Hu, S. Xie, C. Wang and C. Timm, *Beilstein J. Nanotechnol.*, 2017, **8**, 1919.
28 Y. Tsuji, R. Hoffmann, M. Strange and G. C. Solomon, *Proc. Natl. Acad. Sci.*, 2016, **113**, E413.
29 N. Gallagher, H. Zhang, T. Junghoefer, E. Giangrisostomi, R. Ovsyannikov, M. Pink, S. Rajca, M. B. Casu and A. Rajca, *J. Am. Chem. Soc.*, 2019, **141**, 4764.
30 P. Dechambenoit and J. R. Long, *Chem. Soc. Rev.*, 2011, **40**, 3249.
31 H. Zhou, C. C. Mayorga-Martinez, S. Pané, L. Zhang and M. Pumera, *Chem. Rev.*, 2021, **121**, 4999.
32 R. Chiarelli, M. A. Novak, A. Rassat and J. L. Tholence, *Nature*, 1993, **363**, 147.
33 A. J. Banister, N. Bricklebank, W. Clegg, M. R. J. Elsegood, C. I. Gregory, I. Lavender, J. M. Rawson and B. K. Tanner, *J. Chem. Soc., Chem. Commun.*, 1995, 679.
34 A. J. Banister, N. Bricklebank, I. Lavender, J. M. Rawson, C. I. Gregory, B. K. Tanner, W. Clegg, M. R. J. Elsegood and F. Palacio, *Angew. Chem., Int. Ed.*, 1996, **35**, 2533.
35 J. M. Rawson, A. Alberola and A. Whalley, *J. Mater. Chem.*, 2006, **16**, 2560.
36 J. S. Miller, A. J. Epstein and W. M. Reiff, *Science*, 1988, **240**, 40.
37 I. B. Starchenkov and V. G. Andrianov, *Chem. Heterocycl. Compd.*, 1996, **32**, 618 (*Khim. Geterotsikl. Soedin.*, 1996, 717).
38 I. V. Tselinskii, S. F. Mel'nikova, T. V. Romanova, S. V. Pirogov, G. K. Khisamutdinov, T. A. Mratkhuzina, V. L. Korolev, I. Z. Kondyukov, I. S. Abdrakhmanov and S. P. Smirnov, *Russ. J. Org. Chem.*, 1997, **33**, 1656.
39 B. B. Averkiev, A. A. Korlyukov, M. Yu. Antipin, A. B. Sheremetev and T. V. Timofeeva, *Cryst. Growth Des.*, 2014, **14**, 5418.
40 I. B. Starchenkov, V. G. Andrianov and A. F. Mishnev, *Chem. Heterocycl. Compd.*, 1999, **35**, 499 (*Khim. Geterotsikl. Soedin.*, 1999, 564).
41 I. B. Starchenkov and V. G. Andrianov, *Chem. Heterocycl. Compd.*, 1997, **33**, 1219 (*Khim. Geterotsikl. Soedin.*, 1997, 1402).

42 J. Zhang, S. Dharavath, L. A. Mitchell, D. A. Parrish and J. M. Shreeve, *J. Am. Chem. Soc.*, 2016, **138**, 7500.
43 I. B. Starchenkov, V. G. Andrianov and A. F. Mishnev, *Chem. Heterocycl. Compd.*, 1998, **34**, 1081 (*Khim. Geterotsikl. Soedin*., 1998, 1259).
44 C. J. Snyder, L. A. Wells, D. E. Chavez, G. H. Imler and D. A. Parrish, *Chem. Commun.*, 2019, **55**, 2461.
45 H. Gao, Q. Zhang and J. M. Shreeve, *J. Mater. Chem. A*, 2020, **8**, 4193.
46 C. J. Snyder, G. H. Imler, D. E. Chavez and D. A. Parrish, *Cryst. Growth Des.*, 2021, **21**, 1401.
47 I. B. Starchenkov, V. G. Andrianov and A. F. Mishnev, *Chem. Heterocycl. Compd.*, 1997, **33**, 216 (*Khim. Geterotsikl. Soedin*., 1997, 250).
48 I. N. Zyuzin, K. Y. Suponitsky and A. B. Sheremetev, *J. Heterocycl. Chem.*, 2012, **49**, 561.
49 V. G. Andrianov, I. B. Starchenkov and A. F. Mishnev, *Chem. Heterocycl. Compd.*, 1997, **33**, 977 (*Khim. Geterotsikl. Soedin*., 1997, 1120).
50 A. E. Frumkin, N. V. Yudin, K. Y. Suponitsky and A. B. Sheremetev, *Mendeleev Commun.*, 2018, **28**, 135.
51 I. B. Starchenkov and V. G. Andrianov, *Chem. Heterocycl. Compd.*, 1997, **33**, 1352 (*Khim. Geterotsikl. Soedin*., 1997, 1561).
52 I. B. Starchenkov, V. G. Andrianov and A. F. Mishnev, *Chem. Heterocycl. Compd.*, 1997, **33**, 1355 (*Khim. Geterotsikl. Soedin*., 1997, 1565).
53 D. B. Lempert, A. I. Kazakov, A. B. Sheremetev, A. G. Gladyshkin, A. V. Nabatova and L. S. Yanovskii, *Russ. Chem. Bull., Int. Ed.*, 2019, **68**, 1856 (*Izv. Akad. Nauk, Ser. Khim*., 2019, 1856).
54 N. Liu, B. Duan, X. Lu, Q. Zhang, M. Xu, H. Mo and B. Wang, *CrystEngComm*, 2019, **21**, 7271.
55 J.-H. Her, P. W. Stephens, R. A. Davidson, K. S. Min, J. D. Bagnato, K. van Schooten, C. Boehme and J. S. Miller, *J. Am. Chem. Soc.*, 2013, **135**, 18060.
56 H. M. McConnell, *J. Chem. Phys.*, 1963, **39**, 1910.
57 J. J. Novoa, M. Deumal and J. Jornet-Somoza, *Chem. Soc. Rev.*, 2011, **40**, 3182.
58 G. M. Sheldrick, *Acta Crystallogr*., 2015, **C71**, 3.

Received: 6th September 2021; Com. 21/6678